Journal of Sound and Vibration (2002) **253**(5), 941–959
doi:10.1006/jsvi.2001.3944, available online at http://www.idealibrary.com on IDEAL®

A WAVE MODEL FOR A PNEUMATIC TYRE BELT

R. J. Pinnington and A. R. Briscoe

Institute of Sound and Vibration Research, University of Southampton, Highfield, Southampton SO17 1BJ, England. E-mail: rjp@soton.ac.uk

(*Received* 12 *May* 1999, *and in final form* 21 *June* 2001)

A one-dimensional wave equation of an infinite flattened tyre belt is generated. The belt vibration is controlled by bending, tension, shear and the sidewall stiffness. The dispersion relations for two waves in the belt are calculated and used to find both the input impedance and attenuation on a tyre belt of infinite extent. Tension and the sidewall controls the deformation and stiffness below 100 Hz. Waves propagate around the belt above this frequency. The wave speeds due to bending and shear were predicted and measured. The model presented here should be valid for the prediction of tyre response above about 400 Hz when for a car tyre the modal behaviour is observed to cease. In this high-frequency region, the tyre at the input appears to be of infinite extent.

1. INTRODUCTION

Many forms of transportation employ pneumatic tyres to transmit traction, steering and weight from the vehicle to the road surface. The tyre is composed of the belt of stiff wire-reinforced rubber contacting the road surface via the tread; the pressurized air within the tyre cavity and complementary tension in the sidewall sustains the shape, holding the belt in relation to the hub. The sidewall must also transmit the traction to the road surface by internal shear forces.

A rolling tyre vibrates due to fluctuating forces at the interface with the road surface. The vibrations of the tyre carcass radiate sound into the surrounding space, contributing to the external noise of the road vehicle, and also to high-frequency sound inside the passenger compartment. Vibrations are also transmitted through the sidewall and tyre air cavity to the hub, causing low-frequency noise within the passenger compartment via a mainly structural path.

If useful predictions of the vehicle interior and exterior noise are to be made, a dynamic model of the tyre carcass is required to relate the carcass vibration to the input forces at the road interface or contact patch. However, a tyre carcass model is also required to calculate these interaction forces. The first priority therefore in tyre noise prediction is the production of a tyre carcass model.

The tyre vibration problem may be considered in three regimes. At very low frequencies < 100 Hz, a lumped element model [1] is employed to calculate vehicle handling performance. In the mid-frequency range between 100 and 400 Hz, a one-dimensional tensioned Euler beam on a uniformly distributed spring foundation has been used to model the belt and sidewall. The solution of the model gives the resonances and mode shapes of the belt out-of-plane motion [1, 2]. Such a model may be appropriate for vibration transmission to the vehicle but the sidewall and air cavity are not well described.

0022-460X/02/$35.00

At frequencies of the order of 1 kHz, the acoustic half-wavelength corresponds to the belt width permitting the "horn effect" in which sound is radiated very efficiently from the diverging space formed by the belt curvature and the road. The excitation due to tread block impacts, called tread block tones also tend to clump in this frequency regime causing the characteristic broadband hiss of radiated tyre noise. In these high frequencies there is also a contribution to the radiated noise from air displaced and pumped by the tread, but this is a separate mechanism independent of the tyre carcass. A tensioned thick plate model [3, 4] has been developed for this high-frequency regime in which a modal sum was used to solve the orthotropic plate wave equations.

The finite element methods has also been used extensively for the tyre modelling, but this tends to be most appropriate at frequencies below about 400 Hz when modal behaviour is observed and an excessive number of elements are not required [3]. At the more important region around 1 kHz, the damping of the rubber is such that modal behaviour is not observed [1] and so modal methods are not the most appropriate; furthermore, the rubber and stiffening cord material properties are frequency and temperature dependent, tending to stiffen with increasing frequency, adding a further degree of complexity [4].

The intention here is to present a wave model of the tyre in which an equation of motion is satisfied by a set of waves. The model is therefore not so restricted by high frequencies, heavy damping or frequency-dependent material properties. The tyre belt is represented as a tensioned Timoshenko beam upon an arbitrary sidewall impedance which means that the upper frequency is limited by the resonances across the belt depth. In practical terms, this limit would be the first shear resonance of the tread blocks. The tyre is flattened like a snake skin and is of infinite extent in the direction of the belt. This approach is thought to be most appropriate at high frequencies when the damping inhibits modal behaviour and the sound radiation is most significant from the vibration local to the contact patch.

It would not, in principle, be difficult to fit the boundary conditions of a ring to give the lower frequency modes if required, once the various wave types have been identified although the results is only valid above the ring frequency, as curvature is not included in this model.

Out-of-plane motion of the belt is associated with two types of sidewall motion; stretching and flexure. In-plane stretching of the sidewall around the cross-section results in a change in cross-sectional area and couples this mode of carcass vibration to the air space within. These "breathing" waves are important when considering transmission of force to the hub and will be addressed in a latter paper.

The sidewall flexural motion is more noticeable than the stretching motion, although these cause negligible change in cross-sectional area because of the cancellation effect of the opposing motion of half-wavelengths around the section. The structural waves are therefore not well coupled to the air space. Only waves associated with this type of sidewall motion are considered here. First to be considered are the "beam" waves where the motion is uniform across the width, which are designated as $m = 0$, where m corresponds to the number of half-wavelengths across the belt. Only out-of-plane motion is considered, and the possible coupling between out-of-plane and in-plane waves from either belt asymmetry or curvature is neglected.

The wave equation of the model yields dispersion curves of two wave types of each frequency. It is found that the tension controls low-frequency behaviour, bending controls the mid-frequency behaviour and shear the high-frequency behaviour. A comparison is made between the theoretical predictions of wavenumber with some measurements on a stationary tyre.

The model is then extended to consider the higher order modes of the cross-section where $m > 0$. As with any waveguide, there is a "cut-on" frequency below which there is no propagation. Above this frequency the wave speed tends to that of the $m = 0$ wave.

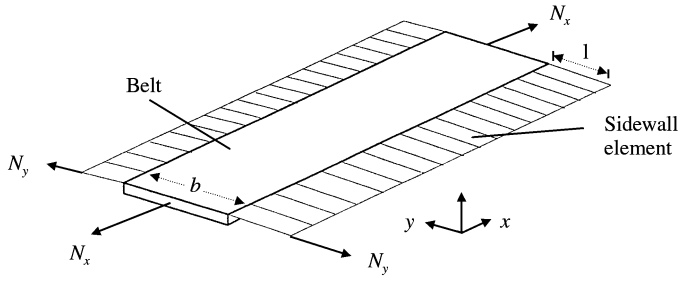

Figure 1. Belt and sidewall model.

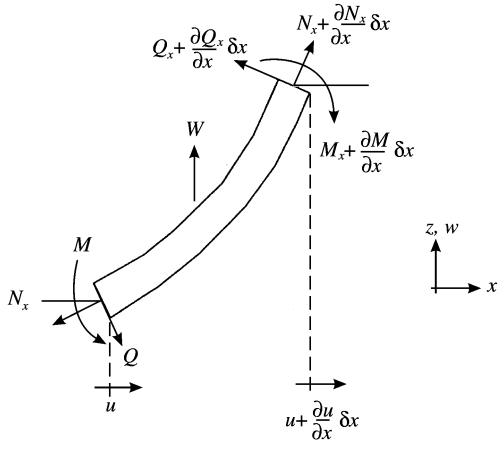

Figure 2. Forces on a section of the belt element in the x direction.

2. THE TYRE MODEL

The tyre dynamics are described by a one-dimensional wave equation. The belt is modelled as a Timoshenko beam to accommodate bending, shear and the rotary inertia effects that are significant at high frequencies. The equations of equilibrium also include the axial tension caused by the air pressure and the in-built prestress. The sidewall is represented as a line impedance in the direction of the tyre circumference, indicated in Figure 1 as the y direction.

The controlling parameters of belt bending stiffness, mass, tension, shear stiffness, rotary inertia and sidewall impedance are represented in non-dimensional form. The dispersion curves relating wavenumbers to the frequency are obtained from the solution of the wave equation. These wavenumbers are substituted back into the equations of equilibrium to give the relative amplitudes of wave types and the transfer functions around the belt.

2.1. THE EQUATIONS OF MOTION OF THE BELT REGION

Consider a section of an infinite Timoshenko beam under tension along the x direction shown in Figure 2.

The tension per width in the beam in the axial direction is denoted by N_x. M and Q are the bending moments and shear forces per unit width acting on the belt section. N_x can be written as

$$N_x = \bar{\sigma}_x h, \tag{1}$$

where h is the beam thickness and $\bar{\sigma}_x$ is the mean axial stress across the section. The bending moment M can be found by integrating the axial stress σ_x weighted by z the distance from the section neutral axis; the belt of thickness h is assumed to be symmetric about the neutral axis:

$$M = \int_{-h/2}^{h/2} \sigma_x z \, \mathrm{d}z = -B_x \frac{\partial^2 w}{\partial x^2}, \tag{2}$$

where B_x is the bending stiffness/width. The out-of-plane displacement w is given by the equation of vertical equilibrium

$$\frac{\partial Q}{\partial x} + N_x \frac{\partial^2 w}{\partial x^2} = \mu_x \ddot{w}, \tag{3}$$

where μ_x is the mass/area of the belt.

Rotational equilibrium of the bending moments and shear stresses yield

$$Q - \frac{\partial M}{\partial x} = \rho I \ddot{\beta}, \tag{4}$$

where ρI_x is the rotary inertia/unit width and β_x is the rotation angle due to bending.

The total rotation of the belt element is the sum of the shear angle α_x plus the rotation angle β_x i.e.,

$$\frac{\partial w}{\partial x} = \alpha_x + \beta_x. \tag{5}$$

The bending moment M is related to the bending angle via equation (2):

$$M = -B_x \frac{\partial \beta_x}{\partial x}. \tag{6}$$

Similarly, the shear force Q is related to the shear angle by

$$Q = S_x \alpha_x, \tag{7}$$

where S_x is the shear stiffness of the belt/width. For a shear modulus G, $S_x = Gh$.

If the above equations (1)–(7) are combined and a harmonic solution of the form $\mathrm{e}^{\mathrm{i}\omega t}$ is applied, the fourth order differential equation of motion is obtained:

$$-\frac{\partial^4 w}{\partial x^4}\left(1 + \frac{N_x}{S_x}\right) + \frac{\partial^2 w}{\partial x^2}\left(\frac{N_x}{B_x} - \frac{\omega^2 \rho I}{B_x}\left(1 + \frac{N_x}{S_x}\right) - \frac{\mu_x \omega^2}{S_x}\right) + w\left(\frac{\mu_x \omega^2}{B_x} - \frac{\omega^4 \rho I \mu_x}{S_x B_x}\right) = 0. \tag{8}$$

The loading of both sidewalls can be included as an impedance/length of Z_s modifying equation (3):

$$\frac{\partial Q}{\partial x} + N_x \frac{\partial^2 w}{\partial x^2} = \mu_x \ddot{w} + \frac{Z_s \dot{w}}{b}, \tag{9}$$

where b is the width of the belt. Equation (8) now becomes

$$-\frac{\partial^4 w}{\partial x^4}\left(1 + \frac{N_x}{S_x}\right) + \frac{\partial^2 w}{\partial x^2}\left(\frac{N_x}{B_x} - \frac{\omega^2 \rho I}{B_x}\left(1 + \frac{N_x}{S_x}\right) - \frac{\mu_x \omega^2}{S_x}\right)$$

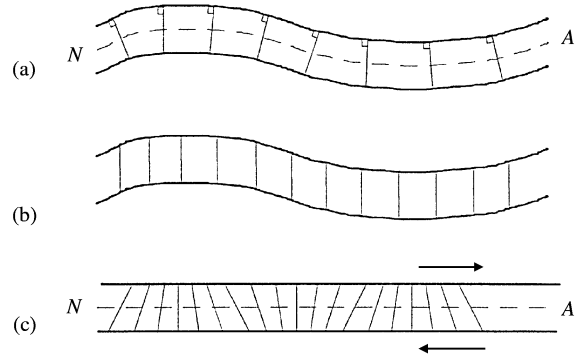

Figure 3. (a) Bending waves; (b) shear waves, (c) rotational waves.

$$+ w\left(\frac{\mu_x\omega^2}{B_x} - \frac{\mathrm{i}\omega Z_s}{bB_x} - \frac{\omega^4\rho I\mu_x}{S_xB_x}\right) = 0. \tag{10}$$

Further simplification of equation (10) is achieved by using the following normalized parameters to describe the tension contribution:

$$\Phi = \frac{N_x}{S_x}, \qquad \chi = \frac{N_x}{B_x}$$

and also the wavenumbers for the four possible propagating waves. The associated deformation patterns are shown in Figure 3. For the tension wave the wavenumber k_{tx} is defined as

$$k_{tx}^2 = \frac{\omega^2\mu_x}{N_x}. \tag{11}$$

This is the wave mechanism of a guitar string in which the restoring force for lateral displacements arises from the tension. This wave can only propagate above the ring frequency in a curved beam, when no in-plane stretching is required.

The wavenumber k_{bx} for bending waves is defined in equation (12) and the associated deformation pattern is seen in Figure 3(a):

$$k_{bx}^4 = \frac{\omega^2\mu_x}{B_x}. \tag{12}$$

The deformation pattern of shear waves is shown in Figure 3(b); these are defined by

$$k_{sx}^2 = \frac{\omega^2\mu_x}{S_x}. \tag{13}$$

Figure 3(c) displays the deformation pattern for a wave which is described here as "rotational"; this is one of the roots of the regular Timoshenko Beam equations. This wave can be seen to be a degenerate bending wave, as there is stretching and compression above and below the neutral axis; there is, however, only in-plane motion without the out-of-plane displacement. This wave could also be described as the first assymetric Lamb wave, the first wave to cut on through the belt depth [5]. The wavenumber is defined by

$$k_{cx}^2 = \frac{\omega^2\rho I_x}{B_x}, \tag{14}$$

which is a function of bending stiffness B_x and second moment of area I'. The mass of the beam section does not appear directly which indicates that there is no section translation in this wave as there is with longitudinal, shear, and bending waves. For symmetrical sections, there is cancellation of the second moment of area within the bending stiffness term and the wavenumber becomes identical to that of the longitudinal wave, i.e.,

$$k_{cl} = \omega \sqrt{\frac{\rho}{E_x}} \tag{15}$$

and is therefore sometimes confused with this wave. For a treaded tyre, however, the asymmetric mass loading will tend to raise the wavenumber. This wave has the possibility of propagating within the tyre contact patch where out-of-plane motion is constrained, and so it may be associated with dynamic phenomena such as tyre squeal.

Equation (10) can now be written as

$$-\frac{\partial^4 w}{\partial x^4}(1 + \Phi) + \frac{\partial^2 w}{\partial x^2}(\chi - (1 + \Phi)k_{cx}^2 - k_{sx}^2) + \left(k_{bx}^4 - k_{sx}^2 k_{cx}^2 - \frac{\mathrm{i}\omega Z_s}{bB_x}\right) w = 0. \tag{16}$$

Substitution of the solution $w = W\mathrm{e}^{-\mathrm{i}kx}$ for a wave propagation in the positive x direction gives a fourth order wavenumber polynomial as would be expected for a Timoshenko beam:

$$k^4(1 + \Phi) + k^2(\chi - (1 + \Phi)k_{cx}^2 - k_{sx}^2) + \left(k_{bx}^4 - k_{sx}^2 k_{cx}^2 - \frac{\mathrm{i}\omega Z_s}{bB_x}\right) = 0. \tag{17}$$

The four roots or rather two pairs of roots are the wavenumber solutions of equation (17).

2.2. WAVENUMBERS FOR AN UNTENSIONED BELT WITH NO SIDEWALL

The wavenumber polynomial in equation (17) is a quadratic in k^2, the solution obtained using a MATLAB program therefore, produces two wavenumber pairs at each frequency. There are three types of waves: propagating, evanescent, and complex, the form of which may be understood by substitution of the wavenumber into the exponential solution of equation (16). Real positive and negative wavenumbers correspond to waves propagating in the positive and negative x directions. The positive and negative imaginary wavenumbers are associated with evanescent waves decaying in the negative and positive x directions. A pair of complex waves gives what appears to be a rapidly decaying standing wave. This last form describes the static deformation pattern dominated by local stiffness effects, for example, when a static load is placed on a compliant surface.

The parameters used in these calculations were measured in reference [4] from samples taken from a car tyre with a tread, at room temperature, and are displayed in Table 1. It is to be noted that apart from the longitudinal elastic modulus, and the loss factors, the other moduli are normalized to the tyre width as presented in the theory. The longitudinal and bending moduli are dominated by the stiffening wires or chords within, while the softer shear moduli are those of the unstiffened elastomers. Three values are given for the shear stiffness on account of the viscoelastic stiffening effect with increasing frequency; the 1 kHz value was used in the modelling. The second moment of area of the asymmetric treaded belt section was calculated by assuming that the neutral axis lay within the mid-plane of the stiffening wires.

Only the positive wavenumbers associated with wave motion is the spacial domain $x > 0$ were plotted on the dispersion curves. Figure 4 shows the first case of an untensioned beam without a sidewall. Below 1 kHz, a bending wave occurs as indicated by the wavenumber

TABLE 1

Material properties

Characteristic	Notation	Tyre part, direction	Static or frequency	Value	Units
Young's modulus	E_x	Belt, x	Static	3·2 E 8	N/m^2
Young's modulus	E_y	Belt, y	Static	7·50 E 8	N/m^2
Bending stiffness/m	B_x	Belt, x	Static	106·9	N m
Bending stiffness/m	B_y	Belt, y	Static	3·8	N m
Bending stiffness/m	B_S	Sidewall	700 Hz	17·0	N m
Tension/m	N_x	Belt, x	Static	5·90 E 4	N/m
Tension/m	N_S	Sidewall	Static	2·00 E 4	N/m
Shear stiffness/m	S_x	Belt, x	100 Hz	6·0 E 5	N/m
Shear stiffness/m	S_x	Belt, x	1000 Hz	3·0 E 5	N/m
Shear stiffness/m	S_x	Belt, x	5000 Hz	1·0 E 6	N/m
Bending loss factor	η_1	Sidewall	Dynamic	Approx. 0·15	—
Shear loss factor	η_2	Belt rubber	Dynamic	Approx. 0·25	—

Note: Second moment of area of the cross-section/width: $I = 10^{-6}\,\mathrm{m}^3$; density of tyre rubber material: $\rho = 1{\cdot}6 \times 10^3\,\mathrm{kg/m}^3$; mass per unit area: $\mu_x = 16\,\mathrm{kg/m}^2$, of main belt; sidewall length = 0·1 m; belt width $b = 0{\cdot}16$ m; and belt diameter $R = 0{\cdot}3$ m.

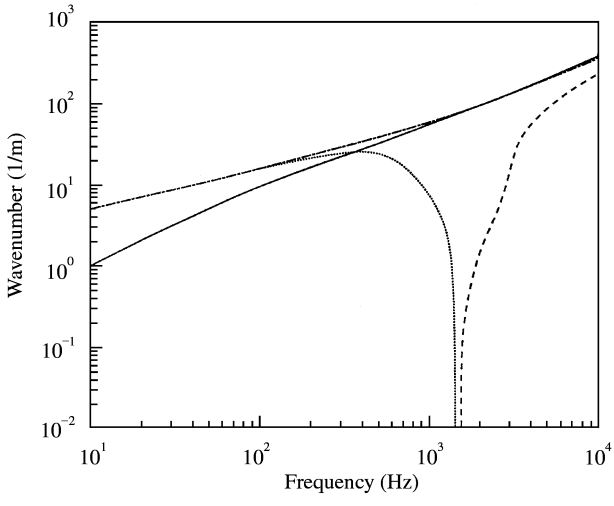

Figure 4. Wavenumbers for a belt without a sidewall: – – – – – – – –, root 1, real, no tension; ---------, root 2, imaginary, no tension; – – – –, root 2, real, with or without tension; ——, root 1, real, with tension.

increase in proportion to $\omega^{1/2}$ in the real root 1. In this frequency range, the bending wavelength is large compared to the cross-sectional dimensions (i.e., the thickness) of the belt and has the deformation pattern seen in Figure 3(a). This frequency-dependent bending wave type travels with a phase speed given by

$$c_B = \sqrt{\omega}\left(\frac{B_x}{\mu_x}\right)^{1/4}. \tag{18}$$

Above 1·5 kHz, the bending wave in real root 1 is superseded by the shear wave; the wavenumber of which is proportional to frequency. The steel cords around the

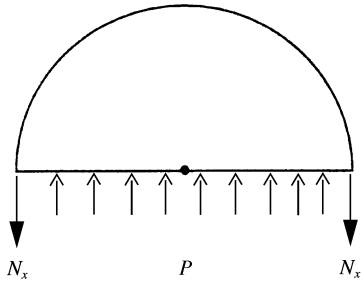

Figure 5. Free body diagram of half-tyre belt.

circumference tend to discourage stretching action occurring during bending allowing the soft intermediate rubber to shear giving the deformation pattern of Figure 3(b). This wave is non-dispersive and travels at a speed of

$$c_{sx} = \sqrt{\frac{S_x}{\mu_x}}. \tag{19}$$

The "rotational" wave (described as real root 2) cuts on 1·5 kHz as seen in Figure 4, its deformation pattern is displayed in Figure 3(c) and its speed is given by

$$c_{cx} = \sqrt{\frac{B_x}{\rho I'}}. \tag{20}$$

Figure 4 also shows the imaginary part of the wavenumber solution (described as imaginary root 2). This corresponds to the evanescent bending wave below 1 kHz. This wave will decay exponentially from the source of vibration but can radiate significant acoustic energy from the excitation area because there is no cancellation from out-of-phase motion.

2.3. WAVENUMBERS FOR PRESSURIZED TYRE WITH NO SIDEWALL

Consider now a pressurized tyre of section seen in Figure 5. The internal air pressure causes a positive tension in both the belt and in the sidewall. The tension in the belt due to the internal pressure can be estimated from the equilibrium of the one-dimensional belt. As the belt is stiffer than the sidewalls their contribution is neglected, and therefore

$$N_x = PR, \tag{21}$$

where R is the radius of the tyre and P is the internal pressure and N_x is the tension/width. A tyre of 0·3 m radius and pressure equal to 2 bar, gives a value of $N_x = 5{\cdot}4 \times 10^4$ N/m. The wave speed of a tension wave increases with tension according to

$$c_{tx} = \sqrt{\frac{N_x}{\mu_x}}. \tag{22}$$

For the chosen parameters, the speed of a tension wave is therefore approximately 60 m/s.

Figure 4 shows the real part of the dispersion relation with the inclusion of tension in the belt equations given above. It can now be seen that the tension wave dominates below 200 Hz and the wave speed is frequency independent. The imaginary wavenumber, not displayed here, is quite large at low frequencies, and is associated with short wavelengths and so is unlikely to be important in tyre dynamics. Above 200 Hz the same behaviour as in

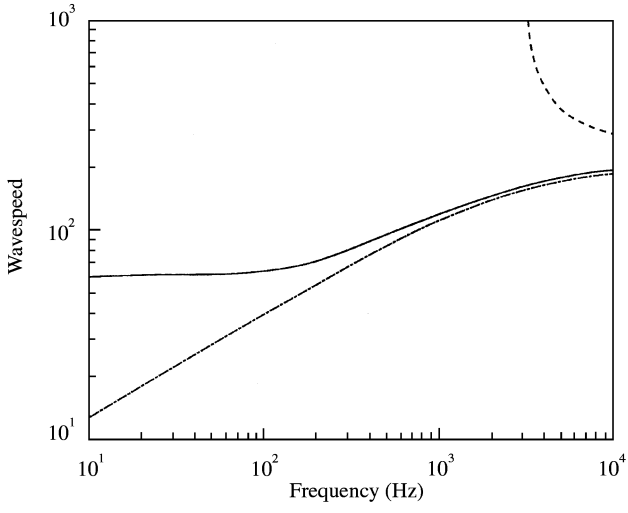

Figure 6. Phase speeds of travelling waves: – – – – – – – –, root 1, real, no tension; ——, root 1, real, with tension; – – – –, root 2, real, with or without tension.

the untensioned belt is observed, which suggests that the flexure dominates the out-of-plane motion. Figure 6 shows a plot of the wave speeds against frequency for these wavenumbers. From this figure it is seen that the tension wave does indeed travel with a phase speed of about 60 m/s below 200 Hz, and then between 200 Hz and 4 kHz the bending wave dominates with a phase speed of about 100 m/s. If there is no tension, the wave speed below 200 Hz is rather slower and frequency dependent. Above 4 kHz, the shear and rotation waves dominate with phase speeds of approximately 200 m/s. It is worth noting that when a tyre is rotated at the phase speed the wave travelling in the counterrotational direction cannot escape the contact zone and so builds into a shock wave, possibly causing the destruction of the tyre. For this particular tyre 60 m/s would then represent the greatest speed achievable.

All the wave speeds are less than the speed of sound in air, and one would therefore only expect sound radiation near the contact patch at the major discontinuities.

3. BELT INPUT MOBILITY

If the power input to a tyre belt is required it is necessary to find the input mobility at the input at $x = 0$. This is obtained by applying a unit normal force/width F and calculating the associated velocity. The two wavenumbers that are found at each frequency are then substituted back into the equations of equilibrium to give the relative wave amplitudes. The absolute amplitudes depend upon the boundary conditions at $x = 0$. For the case considered here a line force/width $F\mathrm{e}^{\mathrm{i}\omega t}$ is applied, and there is a zero slope condition from the symmetry.

By taking a symmetrical section half the normal force on the beam produces a shear force/width, Q_x and a tensile force/width N_x as seen in Figure 7.

The angle θ shown in Figure 7 is composed of two parts described in equation (5); the shear angle α_x and the rotation angle β_x. Equation (5) can be written and expanded as

$$\alpha_x = \sum_{p=1,2} \alpha_{px}\,\mathrm{e}^{-\mathrm{i}k_p x}, \quad \beta_x = \sum_{p=1,2} \beta_{px}\,\mathrm{e}^{-\mathrm{i}k_p x}, \tag{23}$$

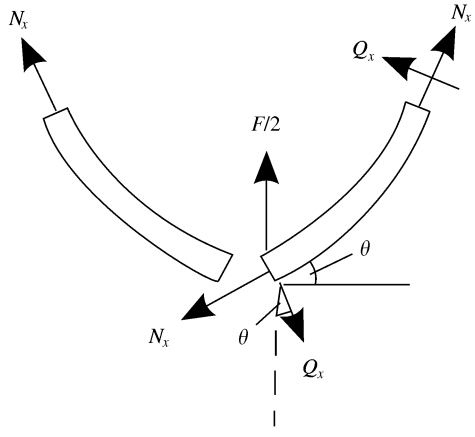

Figure 7. Forces on belt element.

The subscript p denotes a particular wave branch of the dispersion curves corresponding to an axial wavenumber k_p.

The shear force causes shear and bending therefore from equations (4)–(6):

$$Q = S_x \alpha_x = -B_x \frac{\partial^2 \beta_x}{\partial x^2} + \rho I \ddot{\beta}_x. \tag{24}$$

As each wave exists separately, equation (24) can be rewritten using equation (23) as

$$\frac{\beta_{px}}{\alpha_{px}} = \frac{S_x}{B_x} \frac{1}{(k_p^2 - k_{cx}^2)}. \tag{25}$$

The boundary conditions for the vertical force $F/2$ at $x = 0$ are as follows:

(1) $F/2$ resolved into the shear and tension is

$$\frac{F}{2} = -(Q_x \cos\theta + N_x \sin\theta)|_{x=0} \tag{26}$$

which for a small angle θ_x, is

$$\frac{F}{2} = -\left(Q_x + N_x \frac{\partial w}{\partial x}\right)\bigg|_{x=0}. \tag{27}$$

(2) The rotation due to bending is zero, i.e.,

$$\beta_x = 0|_{x=0}. \tag{28}$$

Equations (5), (27) and (28), give

$$\alpha_x = -\frac{F}{2(S_x + N_x)} \tag{29}$$

and by substituting from equation (24) the shear rotation becomes

$$\alpha_x = \frac{B_x}{S_x} \sum_{p=1,2} k_p^2 \beta_{px}. \tag{30}$$

Equations (23), (25) and (30) give the relationship between shear angles for the two waves as

$$\alpha_{2x} = -\alpha_{1x}\left(\frac{k_2^2 - k_{cx}^2}{k_1^2 - k_{cx}^2}\right), \tag{31}$$

where $\alpha_x = \alpha_{x1} + \alpha_{x2}$.

Substitution into equation (31) gives the shear rotation for the first wave type:

$$\alpha_{x1} = -\frac{F}{2(S_x + N_x)}\left(\frac{k_1^2 - k_{cx}^2}{k_1^2 - k_2^2}\right). \tag{32}$$

The radial displacement at any point x is given from equation (5), by integrating with respect to x:

$$w = \sum_{p=1,2} -\frac{1}{\mathrm{i}k_p}(\alpha_{px} + \beta_{px})\,\mathrm{e}^{-\mathrm{i}k_p x}. \tag{33}$$

The out-of-plane velocity $\dot{w}$ at any point x is found by differentiating equation (33) with respect to time and substituting equations (25) and (32) into equation (33):

$$\dot{w} = \frac{\omega F}{2(S_x + N_x)(k_1^2 - k_2^2)}\left\{\frac{1}{k_1}\left[(k_1^2 - k_{cx}^2) + \left(\frac{S_x}{B_x}\right)\right]\mathrm{e}^{-\mathrm{i}k_1 x} - \frac{1}{k_2}\left[(k_2^2 - k_{cx}^2) + \left(\frac{S_x}{B_x}\right)\right]\mathrm{e}^{-\mathrm{i}k_2 x}\right\}. \tag{34}$$

The input mobility, found by setting $x = 0$, is plotted as modulus and real component in Figure 8. The modulus is purely real below 100 Hz when the tension wave dominates and above 2000 Hz where the shear wave is dominant. Between these two frequencies, the bending wave mobility for an infinite belt gives equal real and imaginary components. It may be said then that the displayed mobility is that of an infinite beam in tension below 100 Hz, and the mobility/width is

$$\frac{\dot{w}}{F} = \frac{k_{rx}}{2\omega\mu_x}. \tag{35}$$

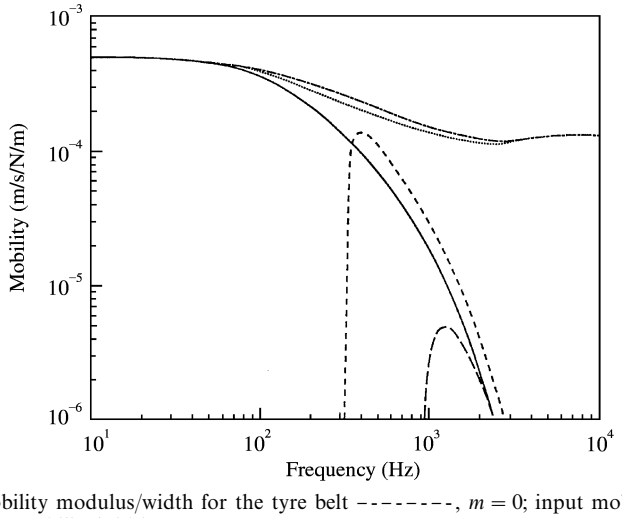

Figure 8. Input mobility modulus/width for the tyre belt – – – – – – – –, $m = 0$; input mobility real component ---------, $m = 0$; transfer mobility/width at 1 m ——, $m = 0$; -----, $m = 2$; – – –, $m = 4$.

Between 100 and 2000 Hz, it is an infinite beam in bending, i.e.,

$$\frac{\dot{w}}{F} = \frac{k_{bx}}{4\omega\mu_x}(1 - \mathrm{i}). \tag{36}$$

Above 2000 Hz, the belt behaves as an infinite belt in shear, i.e., the mobility/width

$$\frac{\dot{w}}{F} = \frac{k_{sx}}{2\omega\mu_x}. \tag{37}$$

The rotational wave will not be greatly excited by the out-of-plane force used here, although it would probably be dominant if a tangential load was applied, as would be the case when tread blocks leave the contact patch of a rotating loaded tyre.

Also plotted in Figure 8 is the transfer mobility at 1 m taken from equation (34), corresponding to the opposite side of the tyre. By 500 Hz the transfer mobility is less than half the input mobility on account of the attenuation due to damping. Significant additive interference of the waves becomes impossible eliminating modal behaviour above 500 Hz. In this region it is therefore adequate to consider the tyre as being of infinite extent.

4. TWO-DIMENSIONAL BELT MODEL

Although the one-dimensional wave, $m = 0$ is probably most significant for sound radiation, higher modes with m half-wavelengths across the belt are also excited by the interaction between the road and the tyre. These are analyzed very approximately here. No attempt is made to model these accurately, as in the real situation these are greatly influenced by the tread pattern. A uniform smooth belt is assumed which supports cross-belt mode shapes of m half-wavelengths, taking a maximum at the outer border to permit coupling with the sidewall. In this assumption it is implicit that the impedance/metre of the belt is greater than that of the sidewall, which is on average true because of the heavier construction of the belt.

The approach here is simply to extend the one-dimensional model as a waveguide allowing higher order modes to cut on and propagate around the tyre. The word "mode" here refers to a cross-belt standing wave pattern with the associated free wave in the circumferential direction. The wave equation for two dimensions can be extended from the non-dimensional expression in equation (8) using a symmetry argument. Bending stiffness B_y, tension N_y and second moment of area in the y direction I_y must be included. u the mass/area and density ρ are unaltered:

$$\begin{aligned} &B_x \frac{\partial^4 w}{\partial x^4}(1 + \phi_x) + B_y \frac{\partial^4 w}{\partial y^4}(1 + \phi_y) - \frac{\partial^2 w}{\partial x^2}\{N_x - B_x(k_{sx}^2 + k_{cx}^2(1 + \phi_x))\} \\ &- \frac{\partial^2 w}{\partial y^2}\{N_y - B_y(k_{sy}^2 + k_{cy}^2(1 + \phi_y))\} + 2B_{xy}\frac{\partial^4 w}{\partial x^2 \partial y^2} \\ &- w(\omega^2\mu - \omega^2\rho I_x k_{sx}^2 - \omega^2\rho I_y k_{sy}^2) = P(x, y). \end{aligned} \tag{38}$$

$P(x, y)$ is the total external pressure acting on the belt. This equation can be rewritten in a more condensed from using the following identities. The non-dimensional parameters are defined as in equation (16), extended to the y direction:

$$\phi_x = \frac{N_x}{S_x}, \qquad \phi_y = \frac{N_y}{S_y},$$

$$B_x' = B_x(1 + \phi_x), \qquad B_y' = B_y(1 + \phi_y),$$

$$T'_x = \{N_x - B_x(k_{sx}^2 + k_{cx}^2(1 + \phi_x))\},$$

$$T'_y = \{N_y - B_y(k_{sy}^2 + k_{cy}^2(1 + \phi_y))\}, \qquad \mu' = (\mu - \rho I_x k_{sx}^2 - \rho I_y k_{sy}^2), \tag{39}$$

$$k_{sx}^2 = \frac{\omega^2 \mu_x}{S_x}, \quad k_{sy}^2 = \frac{\omega^2 \mu_x}{S_y}, \quad k_{cx}^2 = \frac{\omega^2 \rho I_x}{B_x}, \quad k_{cy}^2 = \frac{\omega^2 \rho I_y}{B_y}, \quad k_{bx}^4 = \frac{\omega^2 \mu_x}{B_x}, \quad k_{by}^4 = \frac{\omega^2 \mu_x}{B_y}, \tag{40}$$

Equation (38) can therefore be rewritten more concisely as

$$B'_x \frac{\partial^4 w}{\partial x^4} + 2B_{xy} \frac{\partial^4 w}{\partial x^2 \partial y^2} + B'_y \frac{\partial^4 w}{\partial y^4} - T'_x \frac{\partial^2 w}{\partial x^2} - T'_y \frac{\partial^2 w}{\partial y^2} - \mu' \omega^2 w = P(x, y). \tag{41}$$

The bending stiffnesses B_x B_y are dominated by the presence of the stiffening wires. The cross-modulus B_{xy} is a twist term controlled only by the rubber elastic modulus, which being much smaller than the direct terms is assumed to be negligible here.

The chosen displacement form is $w_m = A \exp(-ik_m x) \cos(k_m y)$ where $k_{mx}x$ is the wavenumber in the x direction and $k_m = \pi m/b$ is the discretized wavenumber in the y direction. The cross-belt displacement patterns are shown in Figure 9, where y is zero on

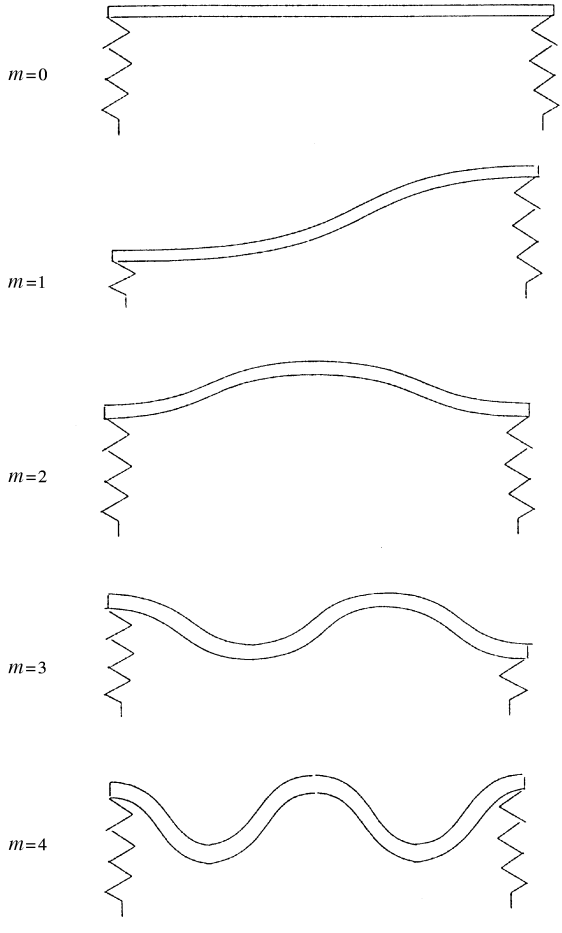

Figure 9. Belt modal deformation patterns.

the midline and extends to $\pm b/2$, where the maximum occurs in the cosine or sine. The even m values therefore take a cosine form and the odd values a sine form.

The displacements $w(x, y)$ and pressure $P(x, y)$ can be written as Fourier expansions:

$$w(x, y) = \sum_{m=0,2,4,\cdots} w_n \cos\left(\frac{m\pi y}{b}\right) e^{-ik_{mx}x} + \sum_{m=1,3,5,\cdots} w_m \sin\left(\frac{m\pi y}{b}\right) e^{-ik_{mx}x}. \quad (42)$$

The pressure from any external forcing function is likewise:

$$P(x, y) = \sum_{m=0,2,4,\cdots} P_m \cos\left(\frac{m\pi y}{b}\right) e^{-ik_{mx}x} + \sum_{m=1,3,5,\cdots} P_m \sin\left(\frac{m\pi y}{b}\right) e^{-ik_{mx}x}. \quad (43)$$

Substitution of solution (42) and (43) into equation (41) yields

$$\left\{B'_x k_{mx}^4 + B'_y \left(\frac{m\pi}{l_y}\right)^4 + T'_x k_{mx}^2 + T'_y \left(\frac{m\pi}{l_y}\right)^2 - \mu'\omega^2 - K_m\right\} w_m = 0. \quad (44)$$

The external force P_m has two components, that which comes from the sidewall and the loading from the road at $x = 0$. If in the first instance the external force from the road is set to zero the component from the sidewall can be identified and included into the left-hand side of equation (44). For zero road loading the right-hand side of equation (44) is now zero, and the fourth order differential equation in k_{mx} is obtained for each mode order m, including the sidewall contribution.

The total pressure per unit belt length $P(x, y)$ only comes from the displacement of the sidewall at $y = \pm b/2$ acting on the sidewall stiffness K_s/length. This is given from equation (42) as

$$P(x, y) = K_s \left[\delta\left(y - \frac{b}{2}\right) + \delta\left(y + \frac{b}{2}\right)\right] \sum_{0,1,2,3} w_m e^{-ik_{mx}x}, \quad (45)$$

where $\delta(x)$ is the Dirac delta function at x.

The coefficients P_m. w_m can be formed from an orthogonality relationship. If equations (44) and (45) are both multipled by $\cos(m\pi y/b)$ and $\sin(m\pi y/b)$ in turn and integrated between $\pm b/2$, i.e., for the cosine

$$\int_{-b/2}^{b/2} P_m \cos^2\left(\frac{m\pi y}{b}\right) dy = K_s \int_{-b/2}^{b/2} \left(\delta\left(y - \frac{b}{2}\right) + \delta\left(y + \frac{b}{2}\right)\right) w_m \cos^2\left(\frac{m\pi y}{b}\right) dy. \quad (46)$$

A similar relation is written for $\sin(m\pi y/b)$. From these two operations, the modal force P_m contribution from the sidewalls is: for $m > 0$, $P_m = 4K_s/b.w_m$ and for $m = 0$, $P_m = 2K_s/b.w_m$.

These values are then inserted back into equation (44) to give for each mode m a similar form to equation (17) as for the $m = 0$ mode. The roots of each equation are obtained in the same way as before.

The resulting dispersion curves, for no sidewall, for $m = 0$, 2, 4, 6 are shown in Figure 10, with only the real wavenumber component displayed. The $m = 0$ waves were discussed earlier and are included for comparison. The $m = 2$ curve begins with a constant section until 300 Hz. This is the real component of a complex pair, the imaginary component has the same magnitude. The complex wave so represented describes the local deformation, with a stiffness controlled characteristic, of the $m = 2$ mode before the propagating wave cuts on. At 300 Hz one flexural wavelength can fit across the belt, as in Figure 9, and the wavenumber theoretically drops to zero. From a comparison with the $m = 0$ case, it can be seen that the newly cut on propagating wave is at the transition between shear and bending. By 1 kHz this wave has almost the same axial wavenumber as the $m = 0$ wave, which means that the $m = 2$ pattern is propagating at the same velocity, i.e., as a shear wave. The $m = 2$

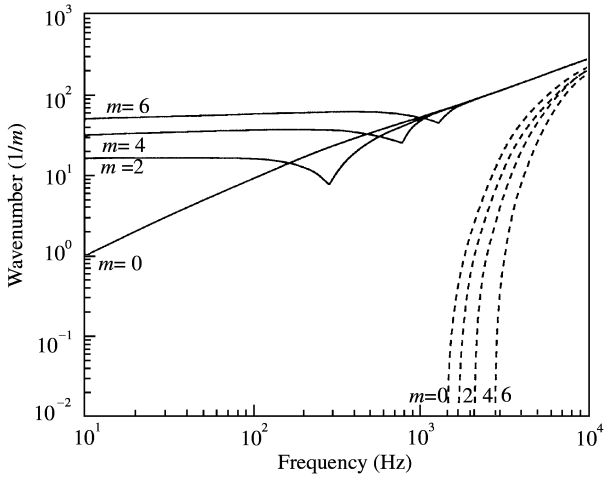

Figure 10. Real wavenumber roots for a tensioned tyre with no sidewall, $m = 0$, 2, 4, 6: ——, root 1; – – – –, root 2.

rotational wave cuts on at 1·5 kHz, at a slightly higher frequency than the cut on of the $m = 0$ rotational wave. Similar observations could be made for the other high order modes. In equation (39), the final term in μ' is omitted as its inclusion gives a negative total inertia at some frequencies, probably at the cut on of cross-belt rotational waves. The exclusion of this effect is unimportant as an accurate modelling is not being attempted in this direction.

If an external force for the mode m, P_m is now applied to the belt at $x = 0$ the displacement response w_m may now be found from equation (44). The modal mobility Y_m is defined as

$$Y_m = \frac{\dot{w}_m}{F_0}. \tag{47}$$

This involves the substitution of the mode m axial wavenumber k_{mx} for the beam axial wavenumber k_x. For the particular example of a point force F_0 applied at $x = 0$ on the midline $y = 0$ the modal forces P_m are given from equation (43), and the modal expansion of a point force, is

$$\frac{F_0}{b}\,\delta(x, y) = \sum_{m=0,2,4,\cdots} P_m \cos\left(\frac{m\pi y}{b}\right). \tag{48}$$

If both sides are multiplied by $\cos(m\pi y/b)$ and integrated between $-b/2 < y < b/2$, the modal forces become

$$P_0 = \left.\frac{F_0}{b}\right|_{m=0}, \qquad P_m = \left.\frac{2F_0}{b}\right|_{m>0}. \tag{49}$$

The modal input mobility/width $b\dot{w}_m(0)/F_0$ can now be found from equation (44) and are plotted in Figure 11. The associated transfer mobilities between the input modal force P_m at $x = 0$ and the velocity 1 m along the belt, are shown in Figure 8. Looking first at the $m = 2$ mode, the input mobility modulus has a stiffness characteristic below the cut on frequency at 300 Hz, and the transfer mobility shows that there is no propagation in this region. Above 300 Hz both the input mobility and transfer mobility for $m > 0$ settle to twice the $m = 0$ values, as expected from equation (49). At 3 kHz a hump indicates the cut on of the rotational wave. Similar observations could be made for the $m = 4$, 6 modes, where the only

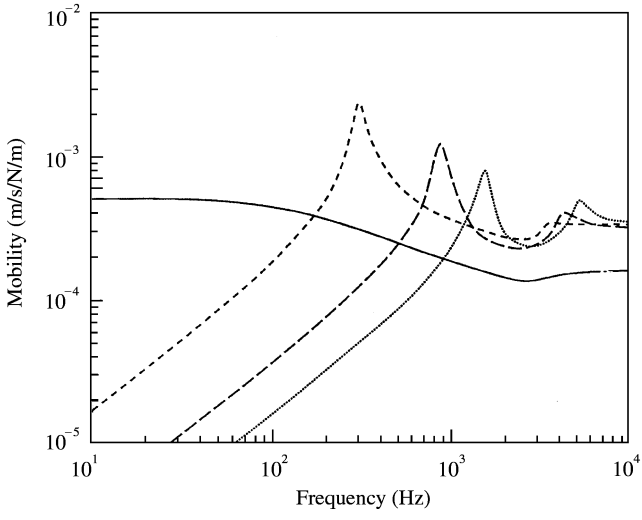

Figure 11. Input mobility modulus/width for a tensioned tyre belt without a sidewall: ——, $m = 0$; -----, $m = 2$; – – –, $m = 4$; ·····, $m = 6$.

difference would be the progressive increase in the cut-on frequencies. As propagation only occurs after the cut on and high attenuation, there would be little standing wave behaviour for these test data. The total point mobility could be obtained by simply summing these modal mobility elements.

5. EXPERIMENTAL DETERMINATION OF WAVE SPEEDS WITHIN A TYRE

An experiment was set up to confirm the theoretical wave speeds and the input mobility. The first stage of this experiment concentrated on measuring the bending wave speeds in an empty treaded tyre. This was achieved using a phase delay method, which is valid when there are only travelling waves present. This condition is achieved when the attenuation is large enough for no circumferential resonances to be seen in the belt, which was above 400 Hz for the tyre used here.

The experimental set-up comprised of a treated (and latter on a treadless) tyre which was freely suspended. The suspension acted as a vibration isolator at frequencies greater than a few Hertz. The tyre was excited radially via a stiff aluminium honeycomb disc (51 mm in diameter) so as to permit mainly one-dimensional $m = 0$ wave propagation around the circumference. To obtain full contact between the tyre and the honeycomb disc, some cement filler was used. It was found from separate experiments that the honeycomb disc excited the tyre width in phase up to 3 kHz. Throughout all the measurements, a broadband random signal was used within the frequency range 0–6·4 kHz. The input fore applied to the tyre was measured using a Kistler type 9041 force guage on the honeycomb disc. The tyre acceleration was measured at several positions using B&K type 4374 accelerometers, which were small enough to fit in the tread close to the belt cords.

Figure 12 shows the experimental set-up for the first method in which two accelerometers are separated by a distance Δx. If a travelling wave occurs in the belt, the phase delay ϕ in travelling a distance Δx between accelerometers $a1$ and $a2$ is

$$\phi = k\,\Delta x, \tag{50}$$

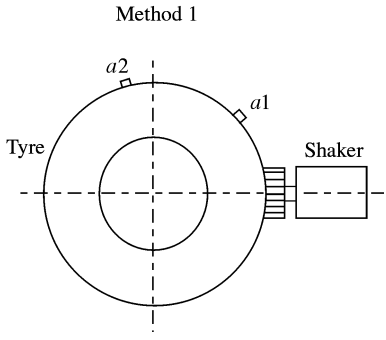

Figure 12. Experimental set-up for determining the bending wave speed using two accelerometers mounted radially.

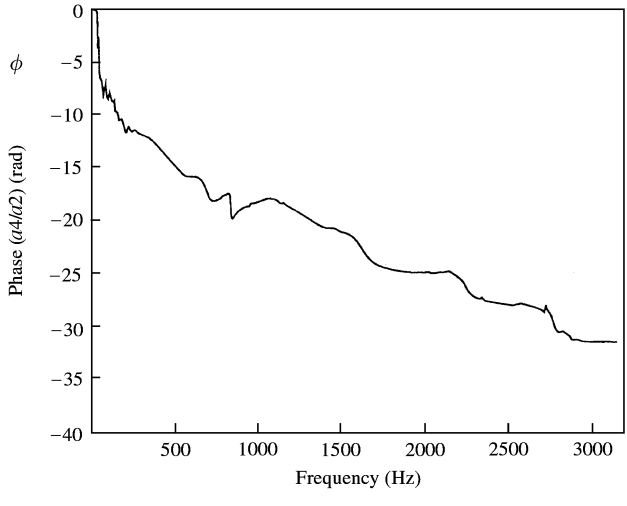

Figure 13. Phase slope obtained from radial measurements on a tyre using two accelerometers.

where k is the wavenumber. For non-dispersive waves where $k = \omega/c_p$ the phase speed is

$$c_p = \frac{\Delta\omega}{\Delta\phi}\Delta x, \tag{51}$$

where $\Delta\phi/\Delta\omega$ is the gradient of the phase diagram. If equation (50) is differentiated with respect to ω

$$\frac{\mathrm{d}\phi}{\mathrm{d}\omega} = \frac{\mathrm{d}k}{\mathrm{d}\omega}\Delta x, \tag{52}$$

the group velocity c_g given as $\mathrm{d}\omega/\mathrm{d}k$ is

$$c_g = \frac{\mathrm{d}\omega}{\mathrm{d}\phi}\Delta x. \tag{53}$$

For non-dispersive waves, equations (51) and (53) are the same. Figure 13 gives the phase ϕ as a function of frequency in Hertz. The plot is fairly smooth until about 700 Hz. The

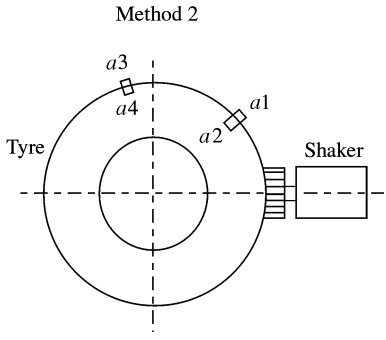

Figure 14. Experimental set-up for determining the bending wave speed using four accelerometers mounted longitudinally.

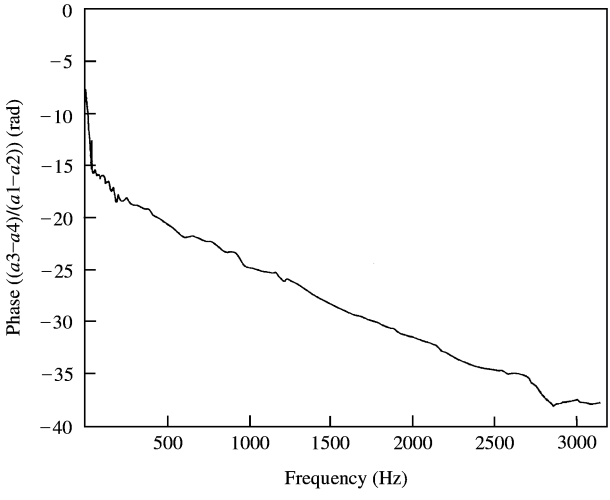

Figure 15. Phase slope obtained from longitudinal measurements on a tyre using four accelerometers.

gradient gives a group velocity of 148 m/s or a phase speed of 74 m/s. Above about 700 Hz, various waves cut on across the belt or new wave types begin as in Figure 3 and the plot becomes unreliable.

To reduce this fluctuation a second method was used, shown in Figure 14 with two pairs of longitudinal accelerometers $a1$, $a2$ and $a3$, $a4$. The signal $a1$ was subtracted from $a2$ eliminating any longitudinal motion of the neutral axis. The signals $a3$, $a4$ were likewise subtracted from each other to give the phase

$$\phi = phase\left(\frac{a3 - a4}{a1 - a2}\right) = k_b \Delta x, \tag{54}$$

Δx was 0·15 m, and the first pair of accelerometers was 0·3 m from the excitation pad. This resulting phase plot is given in Figure 15. Below 500 Hz, the group velocity is given from equation (53) as 140 m/s, corresponding to a 70 m/s phase speed for bending. Above this frequency, a 140 m/s phase speed or group velocity is recorded for the non-dispersive rotational waves monitored. These values agree moderately well with the theoretical values of Figure 6. The data for these predictions was obtained from reference [4] during a measurement programme of tyre properties.

6. CONCLUSIONS

A wave model for a tyre belt was made for both one-dimensional waves and higher order travelling modes which have an integral number of half-wavelengths across the belt. The model included bending, tension, shear and rotary inertia. Sidewalls could be included but are not considered here. The wave types are uncoupled from each other because a symmetrical belt section is assumed.

It was found that tension waves tend to dominate below 100 Hz, and shear waves dominate above 2 kHz. Bending waves are most significant between these extremes. There is also a rotational wave that cuts in at about 2 kHz which travels at speeds close to that of a longitudinal wave. Wave speeds at about 70 m/s were measured and predicted below 500 Hz, and also wave speeds of about 140 m/s were measured and predicted around 2 kHz. The agreement of the wave speeds gives some support for the validity of this model. Realistic loss factors of 0·15 were used in the modelling which suggested that no modal behaviour around the belt could occur above 500 Hz. This means that the infinite model suggested would be valid for predicting sound radiation, which tends to be most significant between 500 Hz and 2 kHz.

REFERENCES

1. W. KROPP 1989 *Applied Acoustics* **26**, 181–192. Structure-borne sound on a smooth tyre.
2. F. BÖHM *Ingenieur-Archiv* **11 966**, 82–103. Mechanik des Gurtelreifens.
3. T. L. RICHARD'S 1991 *Journal of Sound and Vibration* **149**, 235–243. Finite element analysis of structural-acoustic coupling in tyres.
4. K. SMETS 1995 *M.Sc Thesis University of Southampton*. Vibration and wave type recognition in automotive tyres.
5. L. CREMER, M. A. HECKL and E. E. UNGAR 1998 *Structure-borne Sound*. Berlin: Springer-Verlag: second edition.

APPENDIX A: NOMENCLATURE

B_x	bending stiffness/width of the belt ($= B_x(1 + i\eta_1)$)
S_x	shear stiffness/width of the belt ($= S_x(1 + i\eta_2)$)
N_x	tensile force/width of the belt ($= N_x(1 + i\eta_3)$)
μ_x	mass/area
ρ	density of belt material
I	second moment of area of the belt
η_1	bending
η_2	shear loss factors
η_3	tensile loss factor
Z_y	impedance/length

Material losses are introduced using complex modulus term for B_x, S_x, N_x.